CrossMark

Phase Equilibria and Microhardness of As-Cast and Annealed Ni-Al-Os Alloys in Ni-Rich Region

Yan Lin[1] · Ming Wei[1] · Guodong Li[1] · Lijun Zhang[1]

Abstract In this paper, the isothermal section at 1273 K and liquidus projection of ternary Ni-Al-Os system in Ni-rich region were firstly measured by using 6 annealed and 6 as-cast Ni-Al-Os alloys with 65 at.% Ni in combination with x-ray diffraction, optical microscopy and electron probe microanalysis techniques. For the determined partial isothermal section at 1273 K, 2 single-phase, 4 two-phase and 2 three-phase regions were observed. The solubilities of Os in both γ and γ' phases were also determined. For the proposed liquidus projection, four primary surfaces of γ', γ, β and δ, and two invariant reactions were identified. Secondly, the microhardness of both as-cast and annealed alloys were measured. The evolution trend of microhardness in both as-cast and annealed alloys with Os addition generally increases first, and then decreases. Thirdly, the further comprehensive discussion on possible substitution of Re by Os in new-generation nickel-based single-crystal superalloys were performed in terms of strengthening degree, high-temperature creep resistance, and possibility for formation of harmful topologically close-packed phases. It was finally concluded that Os may be used as a new additional element to replace or partly replace Re in Ni-based single crystal superalloys.

Keywords Liquid projection · Microhardness · Ni-Al-Os alloys · Phase equilibria · Re-substitutional element

1 Introduction

Nickel-based superalloys are remarkable for their resistance to mechanical and chemical degradation at temperature up to 1273 K and beyond.[1] The single crystal Ni-based superalloys are widely used to produce the turbine blades and guide vanes for aero-engines and industrial gas turbine due to their high-temperature capability.[1–3] As the operating temperature of gas turbine increases to improve the efficiency, the novel superalloys with better performance are always in need. In past decades, a series of nickel-based single crystal superalloys have been designed with the addition of Re.[4,5] It is well accepted that the creep properties of nickel-based superalloys have been largely improved with the addition of Re. Re not only slows the coarsening process of γ' phase, but also stabilizes the γ' rafted structures. Moreover, the addition of Re also makes the lattice misfit more negative which accelerates the formation of dislocation networks at γ/γ' interfaces. However, the addition of Re makes the microstructural homogenization more difficult during heat treatment.[6,7] What's more, the excessive Re addition could result in the formation of topologically close-packed (TCP) phases.[8–10] The precipitation of TCP phases can deplete the important strengthening elements from the matrix, interrupt the microstructural continuity and degrade the creep properties.[11,12] In order to further improve the microstructural stability and develop the single crystal superalloys to meet higher requirements, development of superalloys with less or even no Re has become a hot topic. One effective strategy lies in the search of the elements with similar or even lower diffusion coefficients in nickel-based matrix in comparison with that of Re.[13–19] Very recently, the diffusion coefficients of Os in nickel-based superalloys at 1573 K were observed in our research group

✉ Lijun Zhang
 xueyun168@gmail.com; lijun.zhang@csu.edu.cn

[1] State Key Laboratory of Powder Metallurgy, Central South University, Changsha 410083, China

to be even lower than those of Re.[15,16] In order to further investigate whether Os can be used as a new additional element to replace or partly replace Re in nickel-base single crystal superalloys, a comprehensive study on phase equilibria and mechanical properties for nickel-base superalloys with Os is the prerequisite. However, the relevant information is still missing in the literature except for binary Ni-Os system.[15]

Consequently, the Ni-Al-Os ternary system is chosen as the target in the present work. The major aims of this paper are (1) to determine the phase equilibria of the Ni-Al-Os system in Ni-rich region by using both annealed and as-cast alloys in combination with x-ray diffraction (XRD) and electronic probe microscopy analyzer (EPMA) techniques; (2) to measure the microhardness for both annealed and as-cast alloys as a function of Os concentration, and (3) to further discuss whether Os is possible to substitute or partially substitute Re in nickel-based superalloys or not.

2 Experimental Procedure

Six ternary Ni-Al-Os alloy samples containing 65 at.% Ni but with different Al/Os ratios were designed. The specimens with nominal compositions listed in Table 1 were prepared by arc-melting the pieces of pure Ni, Al and Os (purities: 99.99, 99.95 and 99.99%, respectively) in an arc melting furnace (WKDHL-I, Opto-electronics Co. Ltd., Beijing, China) under a high purity argon atmosphere, which was equipped with a non-consumable tungsten electrode and a water-cooled copper anode. To ensure

refractory element Os fully integrated into the alloy ingot, the smelting procedure was divided into the following three steps:[15,16] first, the master Ni-Os ingots were melted. After that, the Ni-Os ingots were sheared into small pieces and re-melted several times to ensure the composition homogeneity. In the third step, the appropriate Al content was finally added into each Ni-Os alloy ingot and melted together. During this step, all the ingots were melted repeatedly five times to improve the composition homogeneity. Because the total weight loss for each alloy ingot is less than 1 wt.%, and thus no further composition analysis is needed. Each sample was divided into two pieces. One piece was directly subjected for as-cast analysis, while the other was encapsulated in the evacuated quartz tube for annealing at 1273 K for 52 days to achieve the equilibrium state, followed by water quenching.

The XRD powder measurement of all the samples was performed using a Cu-Ka radiation on a x-ray diffractometer (Rigaku D-max/2550 VB+) at 40 kV and 300 mA to identify the phase structure. After standard metallographic preparation, the samples were examined by optical microscope (Leica DMLP, Wetzlar GmbH, Germany). Then, the microstructure of each sample was examined using the electron probe microanalysis (EPMA) (JXA-8100, JEOL, Japan) in backscattered electron (BSE) imaging mode equipped. Moreover, all the annealed samples were examined by EPMA to determine the composition of each phase. The microhardness of each sample was measured by a microhardness tester (Micromet5104, BUEHLER. Ltd, USA) equipped at maximal load of 9.8 N

Table 1 List of constituent phases and their compositions in the Ni-Al-Os ternary alloys annealed at 1273 K

Alloy	Nominal composition, at.%			EPMA results, at.%*			Phase equilibria
	Ni	Al	Os	Ni	Al	Os	
#1	65	31	4	63.7(4)	35.1(4)	1.15(4)	β
				74.0(2)	25.8(2)	0.15(2)	γ'
				21.4(2)	4.3(22)	74.3(20)	δ
#2	65	25	10	65.6(9)	33.3(9)	1.15(1)	β
				75.7(7)	24.1(7)	0.17(1)	γ'
				15.6(15)	5.3(5)	79.2(26)	δ
#3	65	22	13	75.69(1)	24.12(3)	0.20(2)	γ'
				11.3(14)	4.5(4)	84.2(20)	δ
#4	65	19	16	77.3(2)	21.63(4)	1.1(3)	γ'
				8.5(5)	4.8(18)	86.7(25)	δ
#5	65	15	20	78.4(5)	20.8(4)	0.83(9)	γ'
				84.8(3)	13.7(2)	1.51(5)	γ
				11.7(17)	4.6(3)	83.7(15)	δ
#6	65	5	30	88.9(3)	9.1(3)	1.97(4)	γ
				11.9(6)	0.27(10)	87.9(5)	δ

*The standard deviation of the last significant digit is indicated in parentheses

946

J. Phase Equilib. Diffus. (2018) 39:944–952

to measure the hardness of integrated microstructure. Five measurements were carried out for each sample.

3 Results and Discussion

3.1 Isothermal Section at 1273 K in Ni-Rich Region

Phase equilibria of the Ni-Al-Os ternary system in Ni-rich region at 1273 K were firstly studied on the basis of the samples annealed at 1273 K for 52 days. The obtained experimental information on the phase equilibria in the Ni-Al-Os ternary system is summarized in Tables 1 and 2, and briefly listed as follows.

The microstructure and XRD patterns of alloys #1, #2, and #5 annealed at 1273 K are shown in Fig. 1 and 2. In Fig. 2(a) and (b), the XRD results show that alloys #1 and #2 are in the same three-phase region, consisted of β, γ' and δ phases. In combination with the BSE results, the white, dark gray and pale gray grains in Fig. 1(a) and (b) are δ, γ' and β phases, respectively. The average equilibrium concentrations of Os in γ' phase and β phase of alloys #1 and #2 are measured to be 0.15 at.% and 1.22 at.%. As for alloy #5, the white δ phase, the dark gray γ' phase, and the pale gray γ phase are observed in BSE image in Fig. 1(e) and also confirmed by the XRD patterns in Fig. 2(e). The average concentrations of Os in γ' phase and γ phase are 0.83 and 1.50 at.%, respectively. On the basis of the above results on alloys #1, #2 and #5, the two three-phase regions, $(\beta + \gamma' + \delta)$ and $(\gamma' + \gamma + \delta)$, are confirmed.

The microstructure and XRD patterns of alloys #3, #4 and #6 are also shown in Fig. 1 and 2. It can be seen in Fig. 1(c), (d) and (f) that all these samples contain two phases, i.e. gray γ or γ' phase and white δ phase. The EPMA results indicate that alloys #3 and #4 locate in the two-phase region of $(\gamma' + \delta)$. The solubilities of Os in γ' phase of alloys #3 and #4 are 0.20 and 1.09 at.%, respectively. The micrograph and XRD pattern of alloy #6 displayed respectively in Fig. 1(f) and 2(f) show that the gray γ phase and white δ phase co-exist in this alloy, indicating that alloy #6 locates in the two-phase region of $(\gamma' + \gamma)$.

Based on the above experimental results from all the alloys annealed at 1273 K together with the phase equilibria on the boundary binary Ni-Al[20] and Ni-Os

systems,[21] the isothermal section of the ternary Ni-Al-Os system at 1273 K in Ni-rich region is constructed in Fig. 3. It can be clearly seen that the existence of 2 single-phase regions (γ' and γ), 4 two-phase regions ($\gamma' + \beta$, $\gamma' + \delta$, $\gamma + \gamma'$, and $\gamma + \delta$), and 2 three-phase regions ($\delta + \gamma' + \beta$ and $\gamma + \gamma' + \delta$) can be confirmed at 1273 K.

3.2 Liquidus Projection in Ni-Rich Region

All the samples in as-cast state were also analyzed by XRD and EPMA, and the results are shown in Fig. 4 and 5, respectively, from which a schematic layout of the liquidus projection of ternary Ni-Al-Os system in Ni-rich corner can be constructed.

The XRD pattern of as-cast alloy #1 confirms the coexistence of β phase and γ' phase. Together with EPMA analysis, the gray matrix, the dark gray grains and the light white gray islands in alloy #1 are determined to be β phase, γ' phase and γ phase, respectively. The primary phase is β followed by eutectic reaction involving β and γ. γ' phase is regarded to form via a ternary invariant reaction between residual liquid and β phase. The solidification sequence for alloy #1 is proposed as follows:
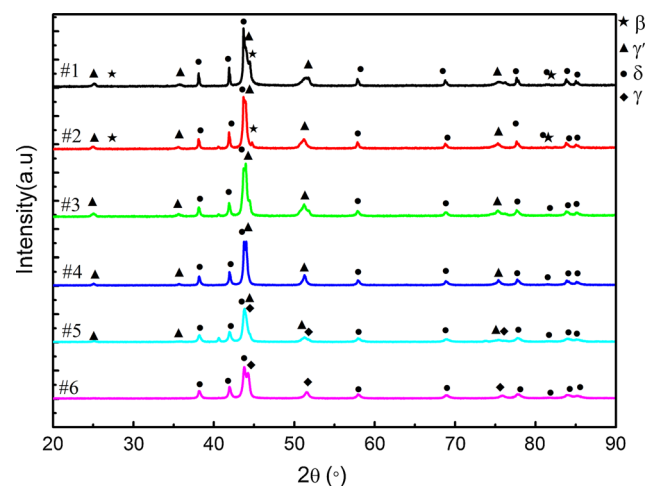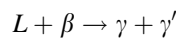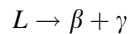
$$L \rightarrow \beta$$
$$L \rightarrow \beta + \gamma$$
$$L + \beta \rightarrow \gamma + \gamma'$$

Fig. 1 XRD patterns of all the alloys (1# ∼ 6#) annealed at 1273 K

Table 2 Ni-Al-Os crystal structure data

Phase	Pearson	Space group	Strukturbericht designation	Prototype
γ	$cF4$	$Fm\text{-}3\,m$	$A1$	Cu
γ'	$cP4$	$Pm\text{-}3\,m$	$L1_2$	Cu$_3$Au
δ	$hP2$	$P63/mmc$	$A3$	Mg
β	$cP2$	$Pm\text{-}3\,m$	$B2$	CsCl

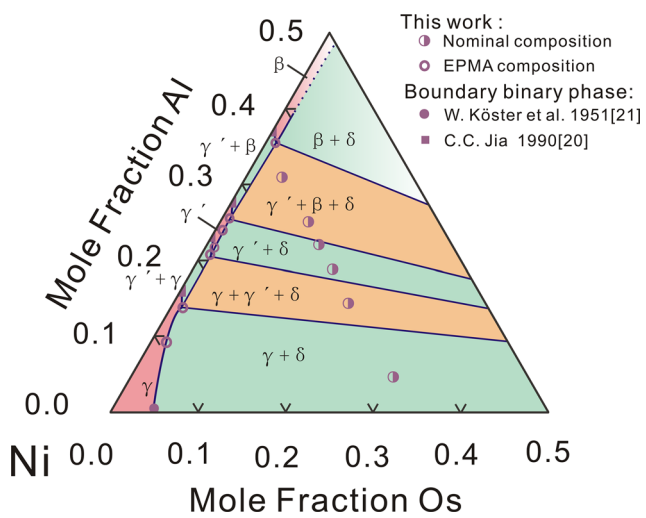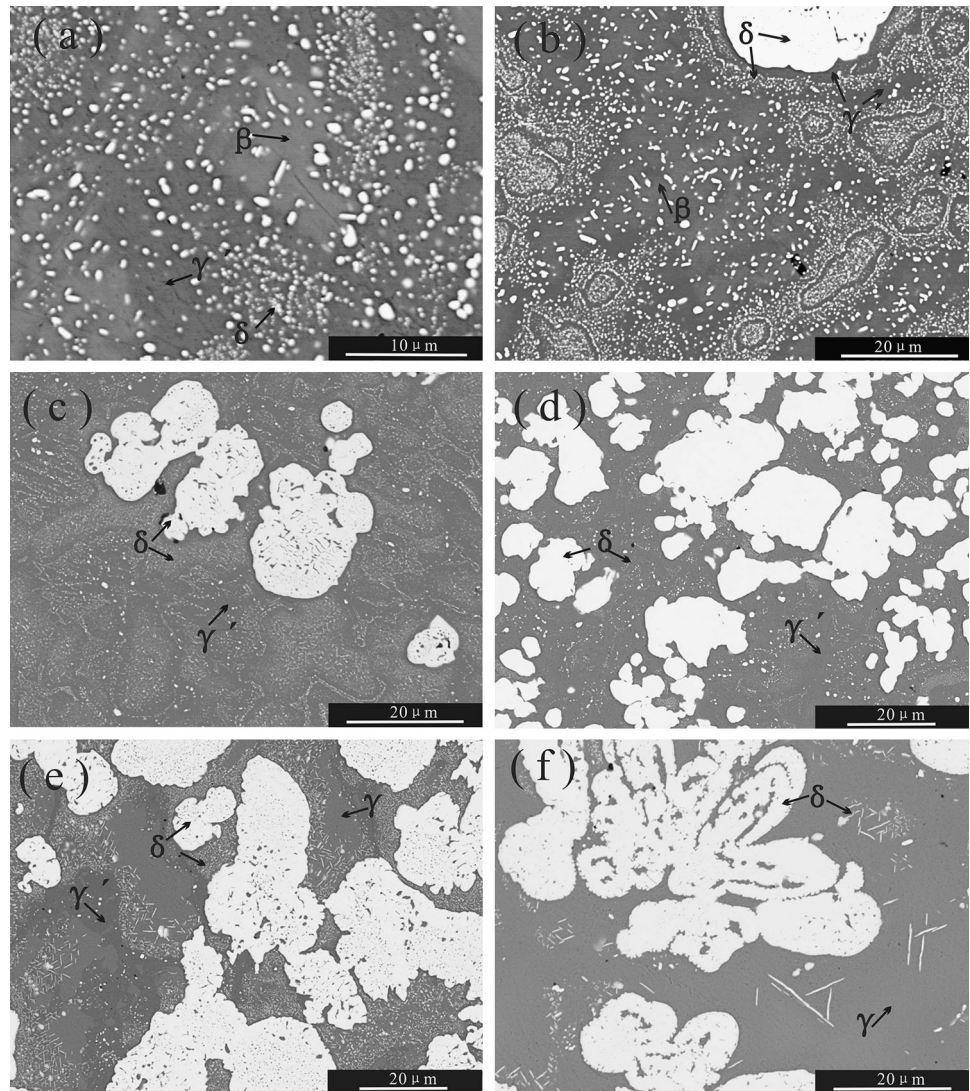Fig. 2 BSE images of the alloys annealed at 1273 K: (a) #1; (b) #2; (c) #3; (d) #4; (e) #5; (f) #6

Fig. 3 Isothermal section of the ternary Ni-Al-Os system at 1273 K in Ni-rich region is constructed. The phase equilibria on the boundary binaries[20,21] were used
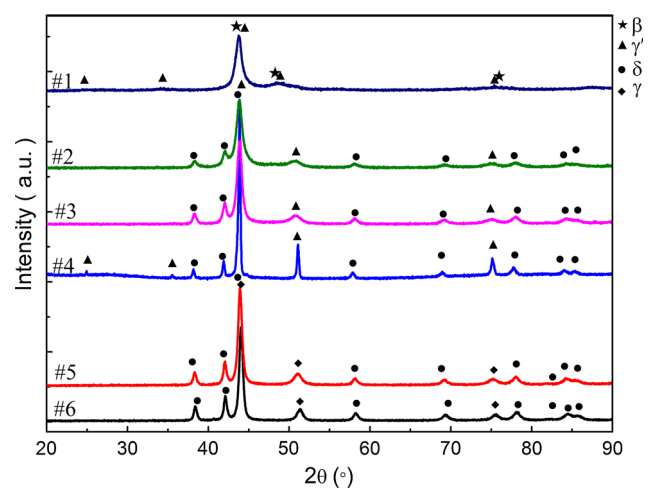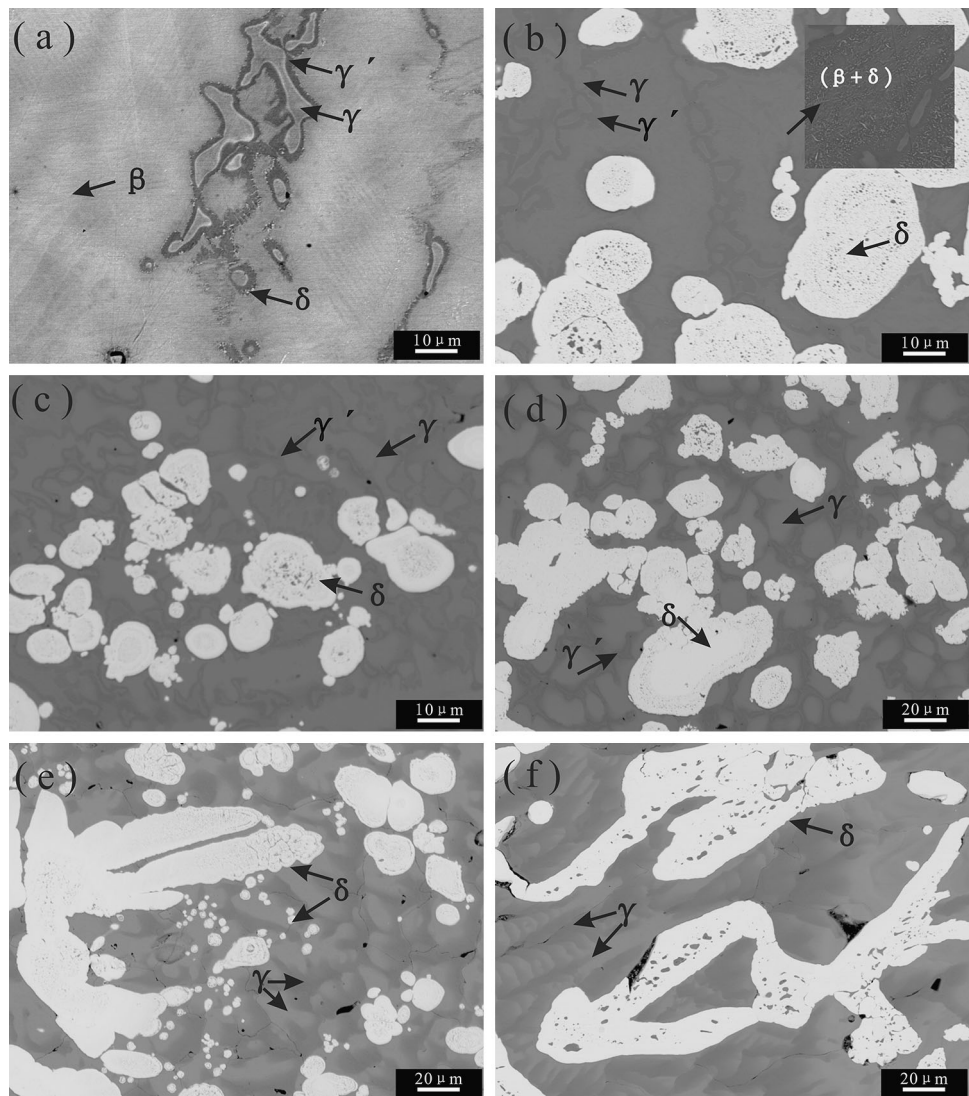
Fig. 4 XRD patterns of all the as-cast alloys (1# ∼ 6#)

948

J. Phase Equilib. Diffus. (2018) 39:944–952

Fig. 5 BSE images of the as-cast alloys: (a) #1; (b) #2; (c) #3; (d) #4; (e) #5; (f) #6

Moreover, there are also some very fine white blocks connecting β phase and γ' phase, which are determined to be δ phase forming as the temperature decreases. From the BSE image shown in Fig. 5(a), the fine white needle-like δ phase can be observed not only along the β grain boundaries but also in β matrix. Thus, it can be roughly concluded that the δ phase precipitates from the β phase.

As-cast alloy #2 owns more complex microstructure with four phases. The XRD pattern of as-cast alloy #2 shows the obvious characteristic peaks of δ and γ' phases. Combined with EPMA analysis, the white phase is determined to be primary δ. The solidification is along the e2-U1-U2 line, and the grey region is the mixture of β phase, fine δ phase, γ' phase, γ phase. Based on the above analysis, the solidification sequence for alloy #2 is given as follows:

$$L \rightarrow \delta$$

$$L \rightarrow \beta + \delta$$

$$L + \delta \rightarrow \beta + \gamma$$

$$L + \beta \rightarrow \gamma + \gamma'$$
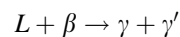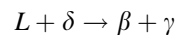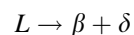
For the transition-type invariant reaction $L + \delta \rightarrow \beta + \gamma$, one can clearly see the primary δ grains surrounded by γ phase from Fig. 5(b), which is a typical peritectic structure. As for the β phase, it forms via binary eutectic reaction, and distributes dispersedly. That is why it is hard to clearly distinguish the peritectic structure.

As-cast alloys #3 and #4 exhibit the similar microstructure. The XRD patterns confirm the existence of δ and γ' phases. Together with EPMA results, the matrix is a mixture of γ phase (grey region) and γ' phase (dark-grey region) because a clear interface between the two phases

exists. Moreover, according to the EPMA analysis, the white islands which are surrounded by γ phase are identified to be primary δ phase. That is because the peritectic process along p2-U1 line is very slow when γ phase has surrounded δ phase. The liquid tends to cross the U1U2p1Nip2 region by forming γ phase directly and arrives at U2p1 line. The solidification sequence for alloy #3 and alloy #4 is proposed as follows:

$$L \rightarrow \delta$$

$$L + \delta \rightarrow \gamma$$

$$L \rightarrow \gamma$$

$$L \rightarrow \gamma + \gamma'$$
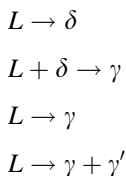
The microstructure of as-cast alloys #5 and #6 are comprised of δ dendrites and occasionally cored γ matrix. Such coring phenomenon occurs when fast cooling does not allow sufficient diffusion to occur to equilibrate the compositional differences between the different layers deposited at lowering temperatures during solidification.[22] The XRD patterns show broad peaks for γ phase since it is cored. Thus, it is deduced that the martix phase in both alloys 5 and 6 is single γ phase based on XRD and EPMA results analysis. In some regions the obviously irregular outline which usually associate with a peritectic reaction appears. In Fig. 5(e) and (f), one can see different morphologies for δ phase, like coarse dendrites and small grains with nearly round shape. This fact indicates that δ phase solidifies from the liquid. The solidification sequence for alloy #5 and alloy #6 is presented as follows:
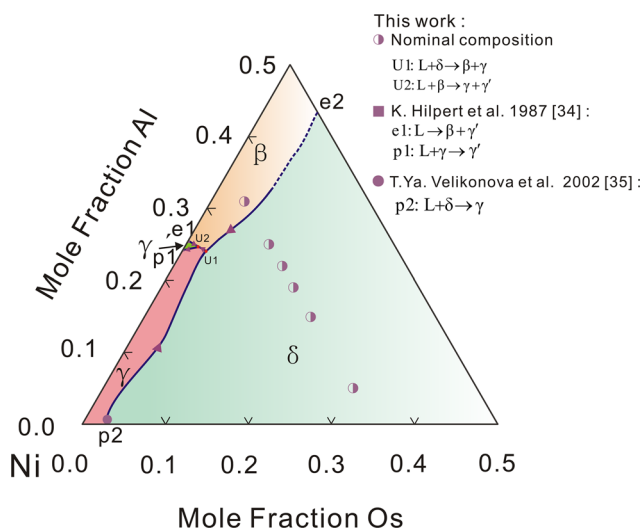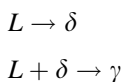
$$L \rightarrow \delta$$

$$L + \delta \rightarrow \gamma$$

Based on the experimental results and analysis above, the liquidus projection of the Ni-Al-Os system in Ni-rich region is constructed in Fig. 6. The alloy compositions are also superimposed. As can be seen, four primary solidification surfaces, i.e., γ', γ, β and δ phases, are contained in the liquidus projection.

3.3 Hardness Behavior

The measured microhardnesses in the as-cast and annealed specimens as a function of Os content are shown in Fig. 7. It can be seen that the hardness shows an obvious change as the increase of Os content. This fact is expected since different contents of Os in the alloys yield very different phases and microstructures, as explained in the previous sections.

Firstly, the highest hardness is observed in the as-cast alloy #2, which can be attributed to the contribution of very fine β/δ eutectic structure. The as-cast alloys #5 and #6, comprised by large γ and δ phases, are with the lowest hardness. The other as-cast alloys are with the moderate/high hardness due to the existence of γ' phase. The highest value observed in the annealed specimens is sample #3 which is constructed of γ' and δ phases. The other annealed alloys are lower than sample #3 due to the decrease amount of γ' phase. In general, the evolution trend of microhardness in both as-cast and annealed alloys with Os addition increases firstly, and then decreases. By coincidence, one can also find that as the Os contents in alloys increases, the content of γ' phase increases firstly, and then deceases, which generally conforms with the trend of microhardness. Thus, one may conclude that the dispersed γ' phase is the mainly strengthening one in all the Ni-rich Ni-Al-Os alloys.
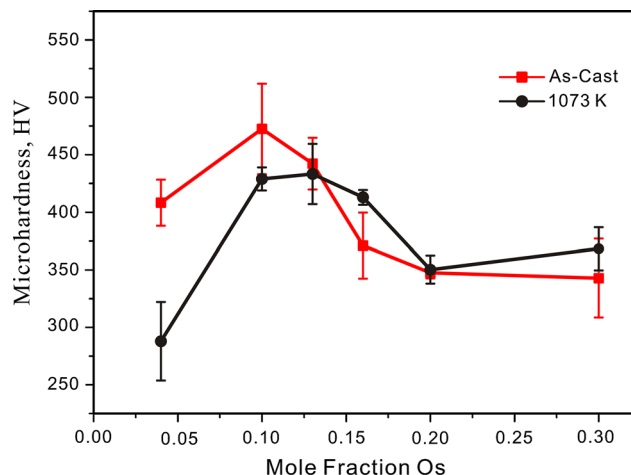
Fig. 6 Liquidus projection of the Ni-Al-Os in Ni-rich region determined in the present work

Fig. 7 Measured microhardness in all the annealed and as-cast alloys as the Os content increases

950

J. Phase Equilib. Diffus. (2018) 39:944–952

Secondly, it can be also observed that the microhardnesses of the as-cast alloys are higher than those of the annealed alloys when the content of Os is lower than 13 at.%, while the microhardnesses of the annealed alloys are higher when the content of Os in alloys exceeds 13 at.%. Thus, besides the effect of γ' phase stated above, the fraction of disperse hard δ-(Os) phase and the grain size should be the other major reasons.

4 Further Discussion on the Possible Substitution of Re

Based on the presently measured partial isothermal section at 1273 K, the maximum solubilities of Os in γ' phase and γ phase are 0.83 and 1.50 at.%, respectively. Due to lack of any experimental data for the ternary Ni-Al-Re at 1273 K, the experimental information of Ni-Al-Re alloys at 1313 K[23] was used instead for direct comparison. In the same two-phase region, the maximum solubilities of Re in γ' phase and γ phase are 1.50 and 2.22 at.%, respectively. Similar with Re that is one of solid solution strengthening elements in nickel-base single crystal superalloys, Os is also more incline to dissolve in γ phase than in γ' phase. Therefore, the fact that Os dissolves in γ phase matrix can also produce the effect of solid solution strengthening in nickel-base single crystal superalloys.

The γ/γ' lattice misfit, usually defined as $\delta = 2(a_{\gamma'} - a_\gamma)/(a_{\gamma'} + a_\gamma)$,[24] is one of the major microstructural characteristics to influence the creep properties in the nickel-based single-crystal superalloys. Consistent with Vegard's law,[1] one can have the relationship, i.e., $a_\gamma = a_\gamma^0 + \sum_i \Gamma_i^\gamma x_i^\gamma$ and $a_{\gamma'} = a_{\gamma'}^0 + \sum_i \Gamma_i^{\gamma'} x_i^{\gamma'}$. The coefficients Γ_{Os}^γ and $\Gamma_{Os}^{\gamma'}$ are 5.99×10^{-4} and 3.47×10^{-4} nm/at.%, respectively. While the coefficients Γ_{Re}^γ and $\Gamma_{Re}^{\gamma'}$ are 4.41×10^{-4} and 2.62×10^{-4} nm/at.%, respectively.[1] The calculated γ/γ' lattice misfit along the phase boundary between $(\gamma + \gamma')$ to $(\gamma + \gamma' + \delta)$ at 1273 K in the Ni-Al-Os system is 2.16×10^{-3}. Similarly, the lattice misfit in the Ni-Al-Re system at 1313 K is 1.94×10^{-3}. The small positive or even negative misfit is beneficial to the high-temperature creep resistance when the service temperature of nickel-base superalloys is more than $0.6 T_m$ (T_m, melting point).[25–27] Here, such small positive γ/γ' lattice misfit is beneficial to the high-temperature creep resistance. Moreover, our previous studies show that the diffusion coefficients of Os in nickel-based superalloys at 1573 K are even lower than those of Re,[15,16] which also indicates that nickel-based single-crystal superalloys with Os own the better the creep resistance.[1] From the above analysis, we infer that Os

addition can improve the high-temperature creep property of nickel-base single crystal superalloys, similar as Re.

Furthermore, we also analyze the possibility for Re-substitution by Os in terms of formation of harmful TCP phases. Generally, the TCP phase is considered as an electronic compound, and the electronic factor is an important criterion to judge the formation of TCP phase. The conventional PHACOMP approach for calculation of average electron vacancy number in γ phase[27–31] has been widely used in the alloy design for nickel-base single crystal superalloys to predict microstructure stability and precipitation trend of TCP phase. The TCP phase tends to precipitate when the average electron vacancy number is larger than the critical value.[27] Moreover, the smaller the average electron vacancy number, the smaller the possibility for TCP formation. The calculated electron vacancy number of element Re is 3.66.[31] While the electron vacancy number of element Os is evaluated to 2.66, which is equivalent to the values of elements Fe and Ru.[27] Considering that the average electron vacancy number of Os is much smaller than Re, the formation possibility for TCP precipitates in nickel-based alloys with Os addition should be smaller than that in nickel-based alloys with Os addition. Furthermore, the previous studies[32,33] have revealed that Ru, which is with the equivalent electron vacancy number as Os, can inhibit the precipitation of TCP phase, and has been included in the new generation of single crystal Ni-based superalloys. Hence, we can also infer that Os addition may also suppress the formation of TCP phase in nickel-base single crystal superalloys.

On one hand, Os tends to dissolve in γ phase as a solution strengthening element like Re, which can improve the strength of alloy. On the other hand, the small positive γ/γ' lattice misfit as well as the lower interdiffusion coefficients in alloys with Os addition are beneficial to improve the creep resistance at high temperatures. Moreover, the formation possibility for TCP phase in alloys with Os addition is also smaller than that in alloys with Re addition. Thus, it is anticipated that Os may be used as a new additional element to replace or partly replace Re in nickel-based single-crystal superalloys.

5 Conclusion

- The isothermal section of the Ni-Al-Os ternary system at 1273 K in Ni-rich region was determined on the basis of the XRD and EPMA analysis results of 6 equilibrated alloys. Two single-phase (γ' and γ), four two-phase ($\gamma' + \beta$, $\gamma' + \delta$, $\gamma + \gamma'$, and $\gamma + \delta$) and two three-phase ($\beta + \gamma' + \delta$, and $\gamma' + \gamma + \delta$) regions were confirmed. Moreover, the solubilities of Os in γ and γ' phases were measured to be limited, and the solubility

of Os in γ phase is slightly larger than that in γ' phase at 1273 K.

- The liquidus projection of the Ni-Al-Os system in Ni-rich corner was constructed by using 6 as-cast alloy together with XRD and EPMA analysis. Four primary solidification surfaces (γ', γ, β and δ) and two ternary invariant reactions were confirmed on the determined liquidus projection.

- The microhardnesses in both as-cast and annealed samples were measured. It was found that the micro-hardness in both as-cast and annealed alloys with Os addition generally increases first, and then decreases. Moreover, the microhardness of the as-cast alloys is higher than that of the annealed alloys when Os addition is lower than 13 at.%, while the microhardness of the annealed alloys is higher when Os addition exceeds 13 at.%.

- The possible substitution of Re by Os in new-generation nickel-based single-crystal superalloys was comprehensively discussed in terms of strengthening degree, high-temperature creep resistance, and possibility for formation of harmful TCP phases. Os addition not only has the tendency to increase the strength and the high-temperature creep resistance, but also the possibility for suppressing the formation of TCP phase. It is finally concluded that Os can replace Re or partly replace Re in new-generation nickel-base single crystal superalloys.

References

1. R.C. Reed, *The Superalloy Fundamentals and Applications*, Cambridge University Press, Cambridge, 2006

2. R.C. Reed, D.C. Cox, and C.M.F. Rae, Kinetics of Rafting in a Single Crystal Superalloy: Effects of Residual Microsegregation, *Mater. Sci. Technol.*, 2007, **23**(3), p 893-902

3. M.V. Nathal and L.J. Ebert, Elevated Temperature Creep-Rupture Behavior of the Single Crystal Nickel-Base Superalloy NASAIR 100, *Metall. Trans. A*, 1985, **16**(3), p 427-439

4. A.F. Giamei and D.L. Anton, Rhenium Additions to a Ni-Base Superalloy: Effects on Microstructure, *Metall. Trans. A*, 1985, **16**(11), p 1997-2005

5. D. Blavette, P. Caron, and T. Khan, An Atom Probe Investigation of the Role of Rhenium Additions in Improving Creep Resistance of Ni-Base Superalloys, *Scripta Metall.*, 1986, **20**(10), p 1395-1400

6. G.E. Fuchs, Solution Heat Treatment Response of a Third Generation Single Crystal Ni-Base Superalloy, *Mater. Sci. Eng. A*, 2001, **300**(1–2), p 52-60

7. M.S.A. Karunaratne, D.C. Cox, P. Carter, and R.C. Reed, Modelling of the Microsegregation in CMSX-4 Superalloy and Its Homogenisation During Heat Treatment, *Superalloys*, 2000, **2000**, p 263-272

8. R. Darolia, D.F. Lahrman, and R.D. Field, Formation of Topologically Closed Packed Phases in Nickel Base Single Crystal Superalloys, *Superalloys*, 1988, **1988**, p 255-264

9. J.X. Yang, Q. Zheng, X.F. Sun, and Z.Q. Hu, Topologically Close-Packed Phase Precipitation in a Nickel-Base Superalloy During Thermal Exposure, *Mater. Sci. Eng. A*, 2007, **465**(1–2), p 100-108

10. C.M.F. Rae and R.C. Reed, The Precipitation of Topologically Close-Packed Phases in Rhenium-Containing Superalloys, *Acta Mater.*, 2001, **49**(19), p 4113-4125

11. C.M.F. Rae, M.S.A. Karunaratne, C.J. Small, R.W. Broomfield, C.N. Jones, and R.C. Reed, Topologically Close Packed Phases in an Experimental Rhenium-Containing Single Crystal Superalloy, *Superalloys*, 2000, **2000**, p 767-776

12. M. Simonetti and P. Caron, Role and Behaviour of μ Phase During Deformation of a Nickel-Based Single Crystal Superalloy, *Mater. Sci. Eng. A*, 1998, **254**(1–2), p 1-12

13. C.L. Zacherl, A Computational Investigation of the Effect of Alloying Elements on the Thermodynamic and Diffusion Properties of fcc Ni Alloys, with Application to the Creep Rate of Dilute Ni-X Alloys. Ph.D. Dissertation, Pennsylvania State University, 2012

14. J. Chen, J.K. Xiao, L.J. Zhang, and Y. Du, Interdiffusion in fcc Ni-X (X = Rh, Ta, W, Re and Ir) Alloys, *J. Alloys Compd.*, 2016, **657**, p 457-463

15. J. Chen, C. Zhang, J. Wang, W.M. Chen, Y. Tang, L.J. Zhang, and Y. Du, Thermodynamic Description, Diffusivities and Atomic Mobilities in Binary Ni-Os System, *CALPHAD.*, 2015, **50**, p 118-125

16. J. Chen, L. Zhang, and X.-G. Lu, Screening of Possible Re-Substitutional Elements in Single Crystal Ni-Based Superalloys: a Viewpoint from Interdiffusion Coefficients in Ni-Al-X Ternaries, *Metall. Mater. Trans. A*, 2018, **49**(7), p 2999-3010

17. R.A. Hobbsa, M.S.A. Karunaratne, S. Tin, R.C. Reed, and C.M.F. Raea, Uphill Diffusion in Ternary Ni-Re-Ru Alloys at 1000 and 1100°C, *Mater. Sci. Eng. A*, 2007, **460**, p 587-594

18. J. Chen and L.J. Zhang, Composition-Dependent Interdiffusivity Matrices in Face Centered Cubic Ni-Al-X (X = Rh and W) Alloys at 1423, 1473 and 1523 K: a High-Throughput Experimental Measurement, *CALPHAD.*, 2018, **60**, p 106-115

19. S.Y. Wen, Y. Tang, J. Zhong, L.J. Zhang, Y. Du, and F. Zheng, High-Throughput Measurements of Interdiffusivity Matrices in fcc Ni-Al-Mo Alloys at 1273-1473 K, *J. Mater. Res.*, 2017, **32**(11), p 2188-2201

20. H. Okamoto, Al-Ni (Aluminum-Nickel), *J. Phase Equilib.*, 1993, **14**(2), p 257-259

21. W. Köster and E. Horn, *Study of Osmium with Cobalt and Nickel, Festschrift aus Anlass des 100-jahrigen Jubilaums der Firma W*, Hanau, C. Heraeus GmBH, 1951, p 114-123

22. L.A. Cornish and M.J. Witcomb, Data Collection for the Calculation of Phase Equilibria, *Mol. Simul.*, 1999, **22**(1), p 57-80

23. S. Miyazaki, Y. Murata, and M. Morinaga, Site Occupancy of Re Atoms in Ni₃Al (γ') and γ-γ' Phase Equilibria in Ni-Al-Re Ternary Alloys, *Tetsu-To-Hagane.*, 1994, **80**(2), p 161-165

24. C. Che, S. Yang, M. Wei, L. Zhang, Q. Li, J. Gao, and Y. Du, Microstructure, Hardness and Interfacial Energy in Co-9Al-10W-xNi (x = 15, 25, 35 at.%) Alloys During Aging, *J. Min. Metall. Sect. B-Metall.*, 2017, **53**(3), p 303-308

25. X.P. Tan, J.L. Liu, T. Jin, Z.Q. Hu, H.U. Hong, B.G. Choi, I.S. Kim, and C.Y. Jo, Effect of Ruthenium on High-Temperature

952

J. Phase Equilib. Diffus. (2018) 39:944–952

Creep Rupture Life of a Single Crystal Nickel-Based Superalloy, *Mater. Sci. Eng. A*, 2001, **528**(29–30), p 8381-8388

26. M.T. Jovanović, V. Maksimović, and I. Cvijović-Alagić, Failure Analysis of Jet Engine Turbine Blade, *Metall. Mater. Eng.*, 2016, **22**(1), p 31-37

27. J.T. Guo, *Materials Science and Engineering for Superalloys*, 1st ed., Science press, Beijing, 2008

28. H.J. Murphy, C.T. Sim, and A.M. Beltran, PHACOMP Revisited, *JOM*, 1968, **20**(11), p 46-53

29. S.P. Rideout, W.D. Manly, E.L. Kamen, B.S. Lement, and P.A. Beck, Intermediate Phases in Ternary Alloy Systems of Transition Elements, *JOM*, 1951, **3**(10), p 872-876

30. L.R. Woodyatt, C.T. Sim, and H.J. Beattie, Prediction of Sigma-Type Phase Occurrence from Compositions in Austenitic Superalloys, *Trans. AIME.*, 1996, **236**(4), p 519-527

31. Q.Y. Shi, Effects of Multiple Alloying Elements on Microstructure and High-Temperature Low-Stress Creep Behavior in Fourth Generation Ni-Based Single Crystal Superalloys. Ph.D. Dissertation, University of Science and Technology Beijing, 2014

32. A.C. Yeh and S. Tin, Effects of Ru on the High-Temperature Phase Stability of Ni-Base Single-Crystal Superalloys, *Metall. Mater. Trans. A*, 2006, **37**(9), p 2621-2631

33. F. Sun and J.X. Zhang, Influence of Ru on the Microstructure of Ni-Base Single Crystal Superalloys, *Adv. Mater. Res.*, 2011, **306–307**, p 562-571

34. K. Hilpert, D. Kobertz, V. Venugopal, M. Miller, H. Gerads, F.J. Bremer, and H. Nickel, Phase Diagram Studies on the Al-Ni System, *Z. Naturforsch. A*, 1987, **42**(11), p 1327-1332

35. T.Ya. Velikonova, T.G. Mazhuga, O.L. Semonova, P.S. Martsenyuk, and V.M. Vereshchaka, Phase Diagram of the Ni-Os System, *Powder Metall. Met. Ceram.*, 2002, **41**(5–6), p 288-295